CAPILLARY DESATURATION CURVE PREDICTION USING 3D MICROTOMOGRAPHY IMAGES

Souhail Youssef, Yannick Peysson, Daniela Bauer , Olga Vizika
IFP Energie nouvelles, 1, avenue de Bois-Préau, 92852 Rueil-Malmaison, France

This paper was prepared for presentation at the International Symposium of the Society of Core Analysts held in St. John's Newfoundland and Labrador, Canada, 16-21 August, 2015

ABSTRACT

In this work, we investigated experimentally the relationship between the *Capillary Desaturation Curve* (CDC) and microscopic properties at the pore scale: the oil cluster size distribution and the porous structure. Experiments were performed on a set of water-wet sandstones with different petrophysical properties. Synchrotron based fast X-ray microtomography was used to capture the dynamics of oil cluster displacements and to get insight into the mechanisms that govern trapped oil mobilization by surfactant injection. Oil cluster size distribution as well as pore geometrical properties were also quantified using lab based microtomography (µ-CT) images at the pore scale. Results showed how the CDC depends on the pore structure and on the oil cluster size distribution at residual oil saturation. We show that rescaling CDC at the macroscopic scale using the relative permeability allows the curves to collapse into one curve. Finally, we propose a new method to predict CDC based on structural properties determined experimentally by µ-CT. We demonstrate, that based on these microscopic properties, the CDC measured on macro plugs can be directly predicted from 3D images.

INTRODUCTION

Enhanced Oil Recovery (EOR) with surfactant can improve significantly the total volume of oil produced from a reservoir. In water-wet reservoirs, at the end of the water flooding, the capillary trapping of the oil phase within the rock micro-structure can lead to a high residual oil saturation. At the pore scale, the oil is trapped at the center of the pores in the form of disconnected droplets or clusters. This remaining oil can be produced if the capillary barrier is suppressed by surfactant injection. In this case, the viscous stresses developed by the water flooding are high enough to mobilize the disconnected oil phase. The evolution of the residual oil saturation as a function of the trapping number N_t (capillary number plus Bond number), is known as the Capillary Desaturation Curve (CDC) and it constitutes an important input parameter in chemical EOR flooding. In this work, we investigate experimentally the relationship between CDC and microscopic properties at the pore scale: the oil cluster size distribution and the porous structure.

In the Oil & Gas area, first attempts to predict CDC from structural parameters have been proposed by Stegemeier [1] or Chatzis *et al.* [2] in the late seventies. They proposed correlations based on the pore throat radii distribution to evaluate the capillary desaturation curve. They obtained, in the domain of application of their correlation, a quite good estimation of measured CDC. However, these approaches using correlations are difficult to extrapolate to other rock types. Yet, these pioneer works show the dependency of CDCs on two main structural parameters: the throat size distribution and the trapped cluster size, which impacts the accessibility path of the flooding fluid. Nowadays, with the renewal of the interest of Chemical EOR methods, new experimental techniques have been developed aiming at the visualization of the oil clusters and the determination of CDC in the case of model porous structures (glass beads or microfluidic network) [3-4]. In the present work we used X-ray tomography [5-7] at two scales (micron and centimeter scale) to provide information on the dependency of capillary desaturation curve with the local microstructure.

MATERIAL AND METHODS

Fluid and Rock Properties

Displacement experiments were conducted using potassium iodide brine KI (4 wt. %) and n-Decane. These two fluids have a significant X-ray absorption contrast, allowing a satisfactory estimation of the two-phase saturations using CT-scan or µ-CT. The interfacial tension between the brine and n-Decane was 40 mN/m. Lower interfacial tension was obtained by adding 0.025 wt. % of Sodium Dodecyl Benzene Sulfonate (SDBS). The interfacial tension between n-Decane and surfactant-brine solution, measured by Spinning Drop method, was 0.3 mN/m. Highly consolidated, water-wet, clean Berea, Bentheimer, Fontainebleau and Clashach sandstones were investigated. Their main petrophysical properties namely permeability (K_0) and porosity (ϕ) as well as the residual oil saturation (S_{or_macro}) are reported in Table 1. S_{or_macro}, are obtained after spontaneous imbibition for at least 72 h. The core is then scanned and then water flooded at very low Nc (7.6 10^{-8}) et re-scanned again to check for the stability.

Table 1. Petrophysical properties of the cores used in coreflood experiments

Core type	K_0 (mD)	Porosity ϕ (%)	S_{or_macro} (%)
Berea	208	19.4	48.2
Bentheimer	2676	22.1	37.2
Fontainebleau	304	11.9	25.0
Clashach	426	14.1	38.4

Core Flood Experiments

Coreflood experiments on macro-plug (33 mm in diameter) were combined with CT-scan imaging to accurately measure the mean residual oil saturation. Samples were first saturated with brine and drained by n-Decane injection using a centrifuge at a Bond number around 10^{-6} . Then, we displaced the oil by injecting brine (or a surfactant added brine) at different capillary numbers and the pressure between the inlet and outlet was continuously measured. More details on experimental procedure and sample properties can be found in [6]. We have also conducted dynamic experiments (drainage, imbibition and surfactant injection) at the TOMCAT synchrotron beam line of the Swiss Light Source (SLS) on a Bentheimer sandstone mini-plug (5.8 mm in diameter and 8 mm in length). 3D images of oil clusters mobilization during the surfactant injection sequence have been captured at different capillary numbers. 3D images were taken with a voxel size of 5 µm and a time interval of 3s. This experiment is described with more details in [8]. Finally mini-plugs (5.6 mm in diameter) of each rock type, were also submitted to drainage under n-Decane by centrifugation followed by a free spontaneous imbibition. Samples were then imaged by a lab µ-CT at residual oil saturation conditions with 3 µm resolution. Porous structure statistics data were determined using the pore extraction methodology developed by Youssef *et al.* [5]. Different structural parameters were computed: pore radii, pore throat radii, pore to throat aspect ratio. 3D volume reconstruction at residual oil saturation conditions permitted then the determination of the oil cluster size distribution for each sample.

EXPERIMENTAL RESULTS

Capillary Desaturation Curves at The Core Scale

Figure 1.a shows the normalized residual oil saturation measured on the four sandstones as a function of the trapping number. Normalized residual oil (S^*_{or}) is expressed by:

$$S^*_{or} = \frac{S_{or}}{S_{ori}} \tag{1}$$

where S_{ori} is the residual oil saturation after the first waterflood (at very low trapping number ~10^{-7}). The trapping number (N_t) is introduced to combine capillary and Bond effect; it is expressed by the following equation :

$$N_t = N_c + N_b \tag{2}$$

where N_c and N_b are respectively capillary number and Bond number given by:

$$N_c = \frac{V\ \mu_w}{\sigma \cos\theta}\ \ ;\ N_b = \frac{\Delta\rho\ g\ K_0 K_{rw}}{\sigma\ \cos\theta} \tag{3}$$

where V is the Darcy velocity, μ_w the viscosity of the brine, σ the oil/brine interfacial tension, θ the contact angle, K_0 the absolute permeability, K_{rw} the brine relative permeability and $\Delta\rho$ the oil/brine density difference.

Residual oil saturation mobilization occurs at trapping number values higher than 10^{-6}. CDC shapes are quite close for all cores. The Fontainebleau sample exhibits a more pronounced slope due to its low S_{ori} plateau. We also observe a significant shift (one decade in N_t) between the decreasing part of all CDC. This shift is attributed to pore structure differences between the samples, since experimental conditions and fluids composition were identical.

Brine Relative Permeabilities at Residual Oil Saturation

Brine relative permeabilities at S_{or} were computed from each imposed flow rate Q and the corresponding measured stabilized pressure difference ΔP by:

$$K_{rw} = \frac{\mu_w}{K_0} \frac{Q}{A} \frac{L}{\Delta P} \tag{4}$$

where A is the section of the plug, L its length, Q the flow rate.

Figure 1.b shows K_{rw} as a function of the trapping number N_t for the different samples. In order to better visualize the curve shape, experimental data were fitted by a polynomial fit. Relative permeability curves are distinct for each sample, their characteristic shape depends on the specific microstructure of the samples. As can be seen, for the low range of trapping numbers, K_{rw} curves remain constant at a low value and independent of N_t. These low values are due to large clusters situated in the center of the pores, that have not yet been mobilized. Then, for higher values of N_t, a strong increase in K_{rw} is observed, that corresponds to the increase of the number of paths accessible to the wetting phase as oil clusters have been evacuated. Once a major part of the oil clusters has been mobilized and evacuated (high N_t values), increase of relative permeability becomes slower and K_{rw} tends to 1. The dependence of K_{rw} on N_t in the intermediate trapping number range stands for the existence of a regime in which the pressure difference does not scale linearly with the flow rate as it is the case for the classical Darcy law. These observations are confirmed by Sinha et al. [9], Tallakstad et al. [10] and Yiotis et al. [11] that investigate steady state immiscible two-phase flow. They observed the existence of three regimes, when expressing the normalized pressure gradient as a function of the capillary number.

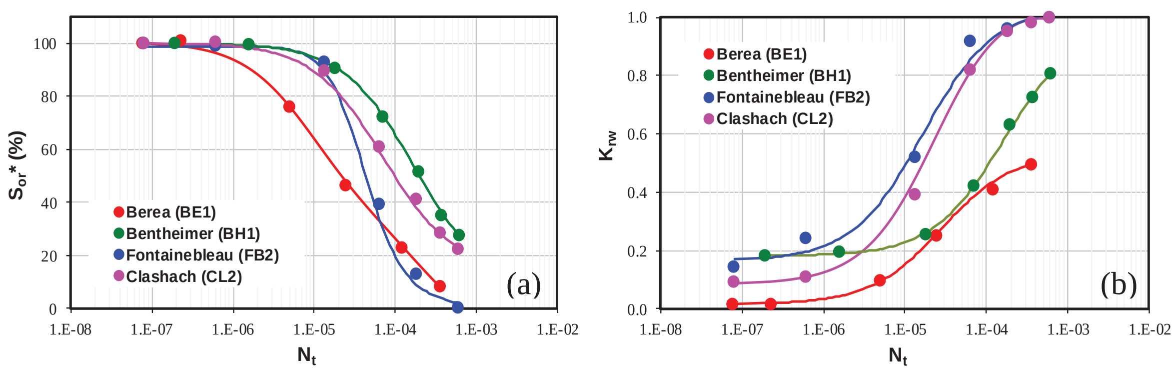

Figure 1: Capillary desaturation curves (a) normalized S_{or} vs. N_t (S_{or} is normalized by S_{ori} which is the residual oil saturation at the end of the waterflood) (b) Brine relative permeabilities as a function of the trapping number N_t for the four sandstones investigated.

Pore Scale Dynamic Observations

To study the behavior of oil clusters during surfactant injection, we have analyzed the size of disconnected oil clusters. These data are extracted from 3D images of the surfactant injection time-series captured during the dynamic experiment described in [8]. In Figure 2.a we report the mean cluster size as well as the size of the largest cluster as a function of the time. The surfactant injection rate was increased each 30 s allowing an increase in the trapping number. This graphic shows that at the beginning of the second and the third stage of surfactant injection at respectively 30 s and 60 s, as soon as the injection rate is increased the size of the largest cluster increases immediately then it decreases to reach almost a constant plateau. This behavior can be explained as follows: once the capillary number has reached a sufficiently high value (critical capillary number) oil cluster menisci begin to move. As the interfacial tension is relatively low, menisci can merge as soon as they get in contact, leading to cluster coalescence and increasing in this way the size of the largest cluster. Afterwards this largest cluster is partially evacuated from the sample and then breaks up in smaller clusters. This is evidenced by Figure 2.b where we can see the evolution of the largest cluster in the time interval from 33 s to 42 s.

In parallel to that, we can see that the mean cluster size decreases rapidly once the capillary number is increased and then converges to a constant value. One important observation is that the level of this plateau decreases for the mean cluster size as well as for the largest cluster size when the capillary number is increased. These observations suggest that statistically the capillary number imposes an upper threshold to the cluster size distribution. This confirms a first order dependency of the cluster size to the capillary number. This point will be developed theoretically in the last part of this paper.

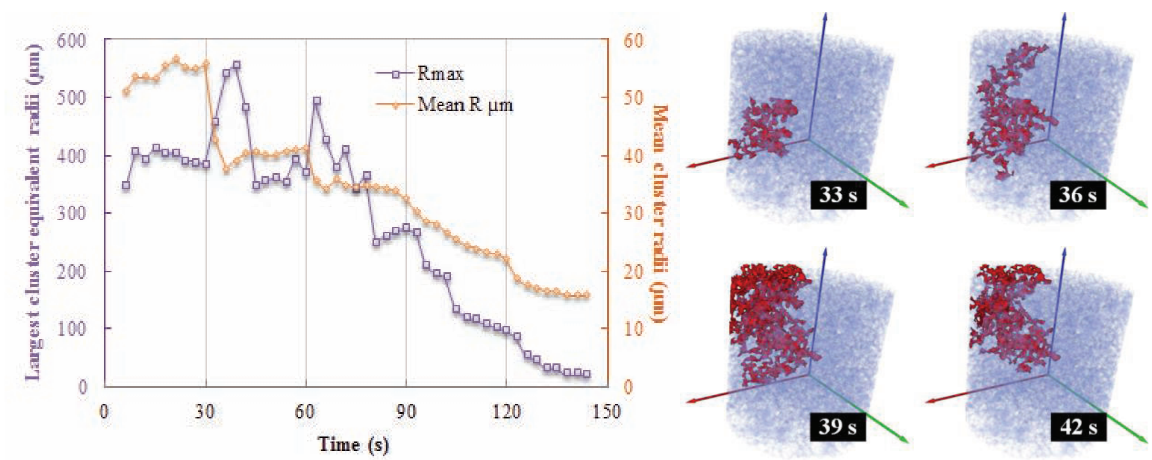

(a) (b)

Figure 2 (a) Evolution of the largest cluster size (R_{max}) and the mean cluster size (R) as a function of the time. (b) Formation and progression of the largest cluster in the time interval from 33s to 42s.

Pore scale statistics

Figure 3 shows 3D images of the four rock types at Sor. Minerals and brine are respectively represented in light gray and dark gray. Oil clusters are represented in color. The color code corresponds to a size classification beginning with the largest clusters in yellow followed by red, green, orange, dark blue and finally the smallest clusters are represented in light blue. The different mean properties computed from these images are reported in Table 2. Image-based porosities are comparable with the macroscopic porosity measurements except for the Clashach sample, certainly due to a local heterogeneity of the sample. The residual oil saturations estimated from the mini-plugs of the samples are systematically higher than those obtained from the macro-plugs (with the exception of the Berea sample where we obtained a similar value). This can be explained by the following fact: spontaneous imbibition of mini-plugs were realized with both faces open, which can create a side effect and increase Sor above the macroscopic value. Finally we also observe that the mean cluster sizes are very close to the mean pore sizes for the four samples.

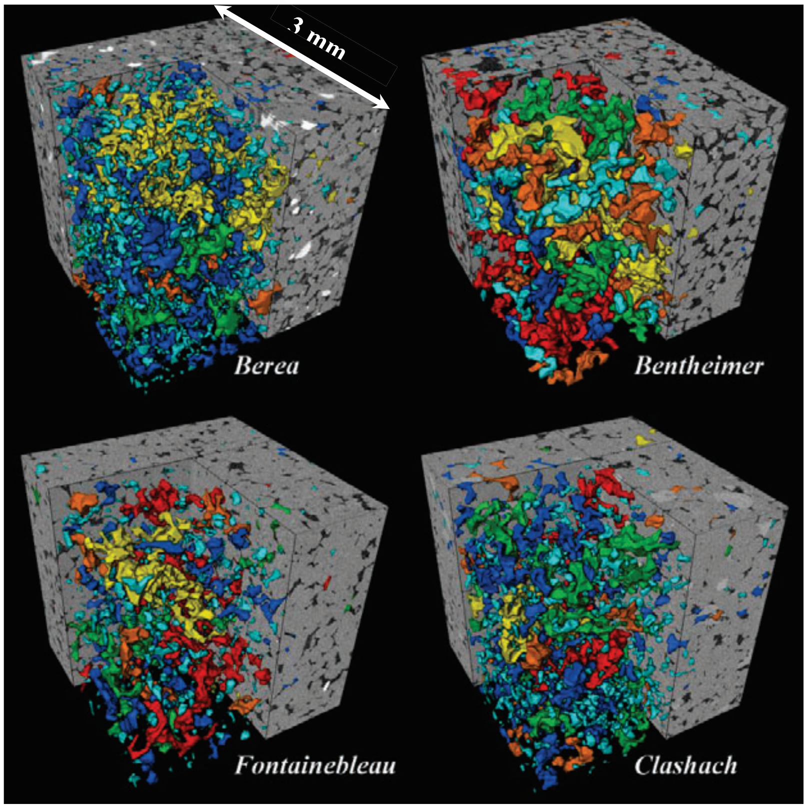

Figure 3: 3D µ-CT images of the four sandstones at residual oil saturation state. Minerals are represented in light gray, brine in dark gray and oil clusters in color. Color code corresponds to a size classification from the largest to the smallest: yellow, red, green, orange, dark blue and light blue.

Table 2. Statistic data of samples used in µ-CT experiments.

Core type	**ϕ_{img} (%)**	**Sor_{img} (%)**	**R (µm)**	**r (µm)**	**R_b (µm)**
Berea	17.6	45.2	28.6	10.5	31.5
Bentheimer	23.1	45.2	36.9	14.8	40.1
Fontainebleau	12.0	37.2	41.4	13.0	38.6
Clashach	10.5	58.2	38.7	12.7	37.2

Figure 4 shows the radius distributions of the oil cluster R_b, pore bodies R, pore bodies containing water and oil and pore bodies containing only water. It can be seen for the four rock types, that mainly small pores contain only water (pink curves). On one hand this is due to the fact that during drainage oil does not invade the smallest pores. On the other hand, water invades pores during spontaneous imbibition in the case of a water wet system in increasing order. The equivalent radius R_b of each oil cluster was computed assuming that the cluster shape is spherical. Mean values of R_b are comparable to mean pore body radii (cf. Table 2) but the largest clusters can extend over hundreds of pores.

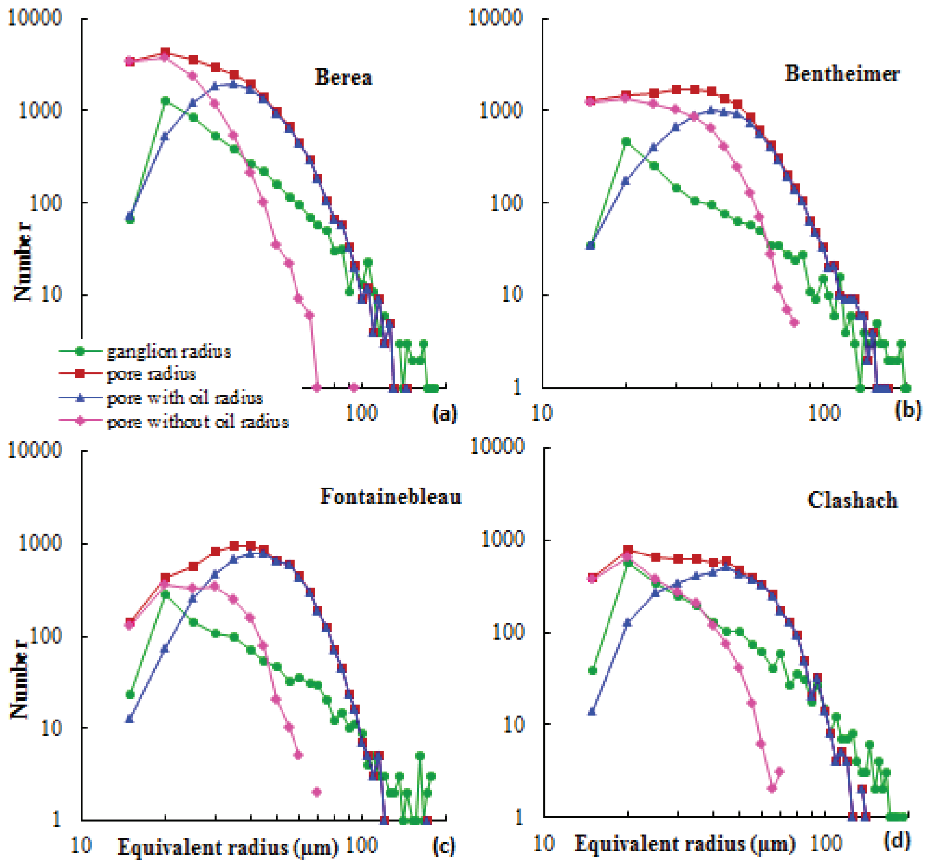

Figure 4: Radius distributions of the oil clusters (R_b), pore bodies (R), pore bodies containing water and oil and pore bodies containing only water (Results are obtained at the mini-plug scale).

Trapping of the oil phase due to spontaneous imbibition might be described by a percolation process [12], as the wetting phase invades first the small pores, leaving disconnected oil clusters in larger pores. Percolation theory suggests that the number of oil clusters of volume *V* follows a power law given by $N(v) \sim v^{-\tau}$ with $\tau = 2.189$. This has been confirmed by Datta *et al.* [13] and Tallakstad *et al.* [10] for glass beads and Iglauer *et al.* [12] for sandstones. They all observed a power law behavior for the range of lower clusters volume followed by an exponential cutoff for larger clusters. We have fitted our data by a power law using a Levenberg-Marquardt algorithm, that is generally used for non-linear fitting problems (cf. Figure 5). We made a cutoff at 100 μm^3 as it is the minimum volume we can measure and found the following exponents: Bentheimer τ=2.37, Berea τ=2.31, Clashach τ=2.05, Fontainebleau τ=2.07. Also, our data seem to show an exponential cutoff, however the number of data points for large clusters is not sufficient to validate this behavior.

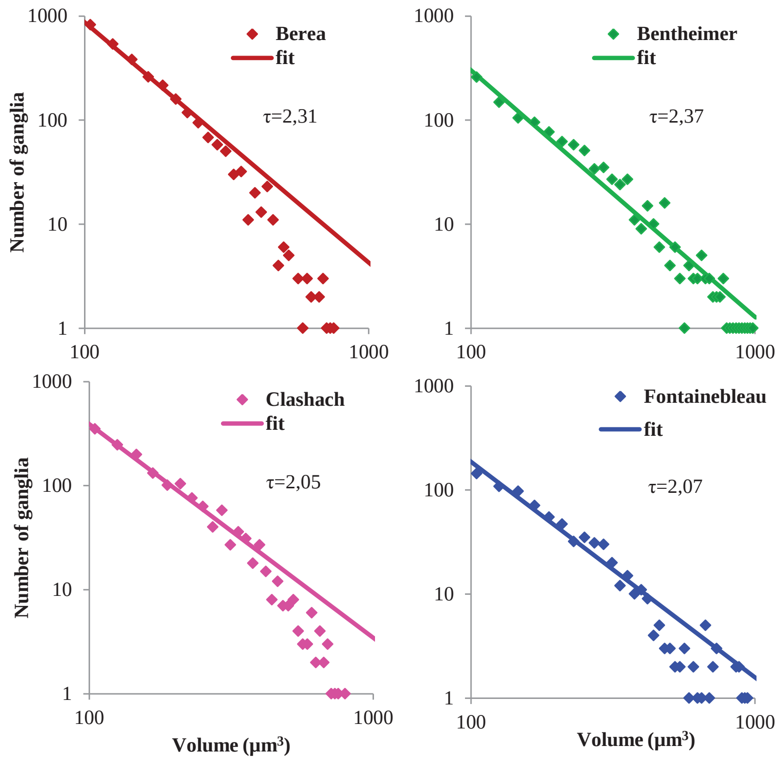

Figure 5: Number of oil ganglia as a function of the ganglia volume and corresponding power law fit. (Results are obtained at the mini-plug scale).

Capillary Desaturation Curve and The Clusters Size Distribution at S_{or}

We have investigated the relation between the clusters size distribution measured at S_{or} and the measured capillary desaturation curve. Figure 6 shows a schematic depiction of an oil ganglion of length $\mathbf{2R_b}$ trapped in a single pore of radius $\mathbf{R}$. The pore is oriented in vertical direction. In the pore, pressure and gravity forces act in the same direction in favor of the mobilization of the oil ganglion through the pore throat (blocking pore throat) of radius $\mathbf{r_p}$, while capillary forces hinder the mobilization.

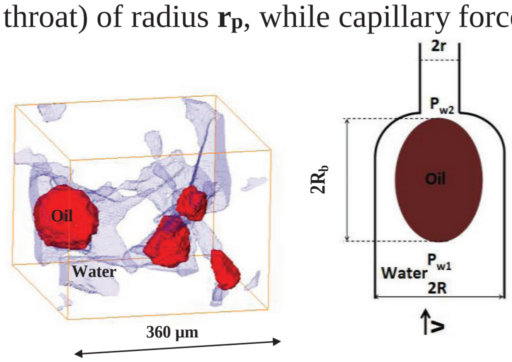

Figure 6: 3D view of trapped oil blobs from Clashach sample and the equivalent pore model scheme.

At the pore scale, we can write a force balance to evaluate the threshold of clusters mobilization [14]. The minimum pressure drop (ΔP_{min}) required to mobilize the oil blob is equal to the Laplace pressure given by:

$$\Delta P_{\min} = \mathrm{P_{w1}} - \mathrm{P_{w2}} - \rho_o \mathrm{g}(2\mathrm{R_b}) = 2\sigma \cos\theta \left(\frac{1}{\mathrm{r_p}} - \frac{1}{\mathrm{R}}\right) \tag{8}$$

where ρ_o represents the oil density, g the gravity acceleration, R the pore radius and r_p the blocking pore throat radius. Darcy's law is expressed by:

$$V = -\frac{K_0 K_{rw}}{\mu \mathrm{L}} (\mathrm{P_{w2}} - \mathrm{P_{w1}} + \rho_w \mathrm{g}\,(2\mathrm{R_b})) \tag{9}$$

where V is the Darcy velocity.

Substituting (P_{w1} - P_{w2}) deduced from equation (9) in equation (8) leads to:

$$\frac{V\mu}{\sigma\cos\theta} + \frac{(\rho_w - \rho_o)\mathrm{g} K_0 K_{rw}}{\sigma\cos\theta} = \frac{K_0 K_{rw}}{\mathrm{R_b}}\left(\frac{1}{\mathrm{r_p}} - \frac{1}{\mathrm{R}}\right) \tag{10}$$

Using the definition of the trapping number equation (10) becomes:

$$N_t = \frac{K_0 K_{rw}}{\mathrm{R_b}}\left(\frac{1}{\mathrm{r_p}} - \frac{1}{\mathrm{R}}\right) \tag{11}$$

As a consequence, and considering $1/r_p >> 1/R$, an oil blob can be mobilized if the following inequality is respected:

$$N_t \geq \frac{K_0 K_{rw}}{\mathrm{r_p R_b}} \tag{12}$$

This equation shows that the trapping number at the threshold of clusters mobilization is linked to three main parameters: the effective brine permeability (K_0K_{rw}), the throat radius of the trapping pores and the clusters size. However, these three parameters are not independent. Indeed, the effective permeability depends on the available path that is controlled at the pore scale by the pore throat radius and the size of the blocking oil cluster. It is also obvious, that during a capillary desaturation process the mean size of the trapped oil cluster changes. Indeed, experimental observations in [7,8,10,14] show that the mean size of the trapped clusters decreases when the capillary number increases during the capillary desaturation process. Equation (5) can be written as:

$$\frac{\mathrm{N_t}}{\mathrm{K_0 K_{rw}}} \geq \frac{1}{\mathrm{r_p R_b}} \tag{13}$$

Parameters of the left hand side of the latter equation are defined at the macro plug scale whereas parameters of the right hand side are defined at the pore scale (mini plug). We now assume that the aspect ratio (α) between the oil cluster radius and the corresponding trapping radius is constant ($r_p = R_b/\alpha$) and multiply the two sides of equation (6) by the square of the mean pore throat radius $< r >^2$. We can then define two equivalent scaling groups :

$$N_t^* = \frac{N_t < r >^2}{K_0 K_{rw}} \geq \frac{\alpha < r >^2}{R_b^2} \quad (14)$$

Figure 7 shows the CDC obtained on macro plugs and plotted as a function of the reduced trapping number. Using this new scaling group the four CDC quasi superimposed with a critical capillary number around $N_t^*=10^{-2}$ and a total desaturation at $N_t^*=1$.

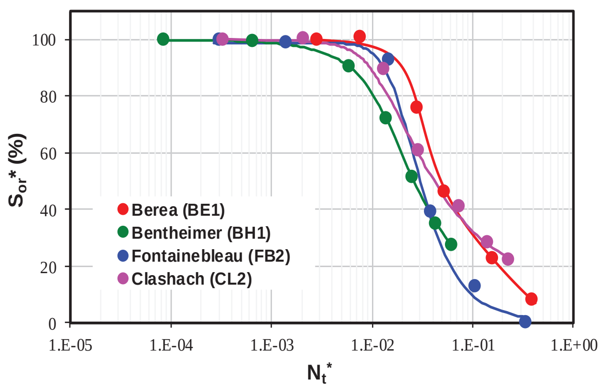

Figure 7 Comparison of capillary desaturation curves plotted using S_{or}^* vs N_t^*. Data are collected on the macro plug experiments for the four sandstones (S_{or}^* is the residual oil saturation normalized by the residual oil saturation after the first waterflood, see [6] for the experimental details).

According to equation (13) we can consider that after flooding at a given reduced trapping number N_t* all the clusters with a size greater than R_b are removed. At this trapping number the normalized residual oil saturation $S^*_{or}(N_t^*)$ in the mini plug can be expressed as:

$$S_{or}^*(N_t^*) = \frac{4\pi}{3V_{ori}} \sum_{R_{bi} \leq R_b} R_{bi}^3 f(R_b = R_{bi}) \quad (15)$$

where R_{bi} is the ith class size of ganglion radius distribution function f(R_b) and V_{ori} is the total volume of oil in the mini plug after spontaneous imbibition. One can notice that the function S^*_{or} (N_t*) is the volume weighted cumulative function of the ganglion size distribution. In Figure 8 we plot S^*_{or} obtained on macro plugs as a function of $\frac{N_t < r >^2}{K_0 K_{rw}}$ and S^*_{or} obtained by equation (15) as a function of $\frac{\alpha < r >^2}{R_b^2}$ which correspond respectively to the CDC at the macro and mini plug scale.

For this study we consider that α is constant. The aspect ratio α is computed from the ratio between $<R_b>$ and $< r >$, supposing that $< r > \sim < r_p >$ as $< r_p >$ cannot be obtained easily from the μ-CT images since the flow direction is not known.From these curves we can see that the CDCs defined at the two different scales match very well for all samples. These results show that CDCs can be estimated using structural parameters and that ganglion size distribution is a first order parameter.

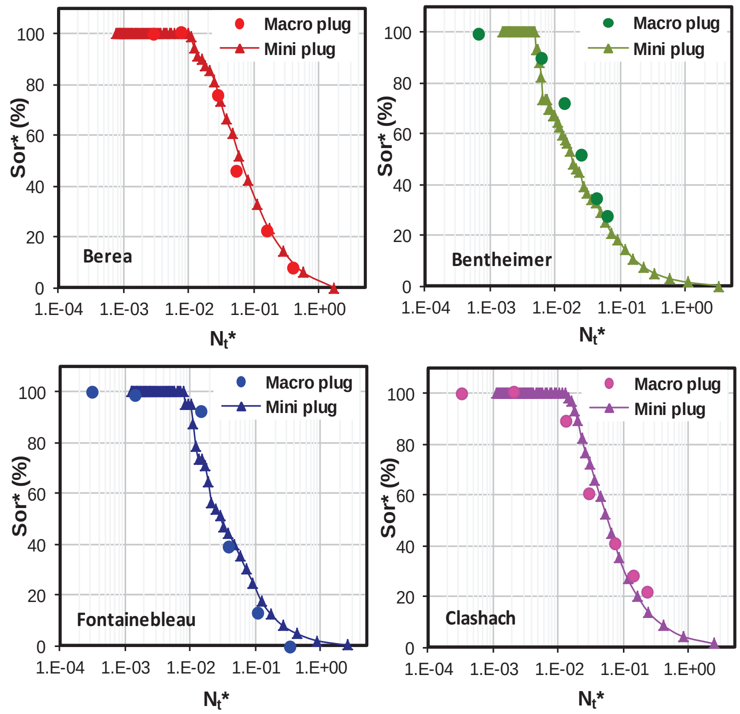

Figure 8: Capillary desaturation curves as a function of the modified trapping number (from macro plug experiments (points) and from mini plug image properties computed at Sor (triangles).

CONCLUSION

In the present work, we performed brine and surfactant flooding experiments in Berea, Bentheimer, Fontainebleau and Clashach sandstone in order to investigate the influence of the pore structure on the mobilization of oil clusters. X-ray Computed Tomography at two scales was used to provide information on the rock local microstructure and to measure the mean residual oil saturation at different trapping number values. A modified trapping number was introduced, that takes into account effective brine permeability, or, in other words, the size of the effective pathways through which fluid flow occurs. Use of the modified trapping number permits rescaling CDC on quasi unique curves. Experimental results showed that by using pore scale geometrical properties extracted from 3D X-ray images we were able to predict satisfactorily the capillary desaturation curve for the different samples from the size distribution of the trapped oil at initial residual saturation. Our observation highlights the importance of the initial distribution of disconnected oil clusters to understand the properties of capillary desaturation curves. From the observation of the relative permeability variation with the trapping number for all rock types, we deduced also a specific scaling for the trapping number. All these results give new insights in recovery mechanisms and interpretation of capillary desaturation of a discontinuous non-wetting trapped phase in a porous media. Introducing this new experimental approach in a chemical EOR process design allows to save time compared with conventional core flood methods and gives valuable information on the rock properties at the early beginning of the workflow.

REFERENCES

1. Stegemeier, G.L., Mechanisms of Entrapment and Mobilization of Oil in Porous Media, D.O. Shah and R.S. Schechter, Editors, *Improved Oil Recovery by Surfactant and Polymer Flooding*, Academic Press, Inc., New York, 55-91, (1977)

2. Chatzis I., Morrow N.R., Lim H.T., Magnitude and detailed structure of residual oil saturation SPEJ, 23 (2), 311-326, SPE-10681-PA, (1983)

3. Krummel A.T., Datta S.S., Munster S., Weitz D.A. Visualizing Multiphase Flow and Trapped Fluid Configurations in a Model Three-Dimensional Porous Medium. *AIChE Journal*, 59: 1022-1029, (2013)

4. Romano M., Chabert M., Cuenca A., and Bodiguel H., Strong influence of geometrical heterogeneity on drainage in porous media, *Phys. Rev. E,* 84: 065302, (2011)

5. Youssef S., Rosenberg E., Glan N., Bekri S., Vizika O., Quantitative 3D characterization of the pore space of real rocks : improved µ-CT resolution and pore extraction methodology, SCA2007-17, *Int. Sym. of the Society of Core Analysts,* Calgary, Canada (2007)

6. Oughanem, R., Youssef S., Peysson Y., Bazin B., Maire E., and Vizika O., Pore-scale to core-scale study of capillary desaturation curves using multi-scale 3D imaging, SCA2013-27, *Int. Sym. of the Society of Core Analysts*, Napa Valley, *California (2013)*

7. Berg S., Armstrong R., Ott H., Georgiadis A., S. Klapp A., Schwing A., Neiteler R., Brussee N., Makurat A., Leu L, Enzmann F., Schwarz J.-O., Wolf M., Khan F., Kersten M., Irvine S., Stampanoni M., Multiphase flow in porous rock imaged under dynamic flow conditions with fast x-ray computed microtomography, *SCA2013-11, Int. Sym. of the Society of Core Analysts*, Napa Valley, *California (2013)*

8. Youssef S., Rosenberg E., Deschamps E., Oughanem R., Maire E., Mokso R., Oil clusters dynamics in natural porous media during surfactant flooding captured by ultra-fast x-ray microtomography, SCA2014-23 *Int. Sym. of the Society of Core Analysts, Avignon, France (2014)*

9. Sinha, S. and A. Hansen: "Effective rheology of immiscible two-phase flow in porous media," *Europhysics Letters* (2012), 1-5

10. Tallakstad K.T., Knudsen H.A., Ramstad T., Løvoll G., Maløy K.J., Toussaint R., and Flekkøy G.E., Steady-state, simultaneous two-phase flow in porous media: An experimental study, *Phys. Rev. E,* 80: 036308, (2009)

11. Yiotis, A.G., Talon, L., Salin, D.: Blob population dynamics during immiscible two-phase flows in reconstructed porous media. *Phys. Rev. E,* 87, (2013)

12. Iglauer S., Favretto S., Spinelli G., Schena G., and Blunt M.J., X-ray tomography measurements of power-law cluster size distributions for the non-wetting phase in sandstones, *Phys. Rev. E,* 82: 056315 (2010)

13. Datta S.S, Ramakrishnan T.S., David A. and Weitz D.A. Mobilization of a trapped non-wetting fluid from a three-dimensional porous medium. *Phys. Fluids* 26: 022002, (2014)

14. Lenormand, R. and Zacone C., Physics of Blob Displacement in a Two-Dimensional Porous Medium, *SPE Formation Evaluation*, 3 (1): 271-275, (1988)